Chemical Geology 674 (2025) 122531

Contents lists available at ScienceDirect

Chemical Geology

journal homepage: www.elsevier.com/locate/chemgeo

Removal of arsenate from aqueous solutions by transformation of cerussite to mimetite

Ewa Stępień [a,*], Maude Julia [b], Daniel Buczko [c,d], Martina Bottaro [e], Andreas Kappler [e], Maciej Manecki [a,c], Christine V. Putnis [b,f]

[a] Faculty of Geology, Geophysics and Environmental Protection, AGH University of Krakow, al. Mickiewicza 30, 30-059 Kraków, Poland
[b] Institut für Mineralogie, University of Münster, Corrensstrasse 24, 48149 Münster, Germany
[c] Department of Earth Sciences, Uppsala University, Villavägen 16, SE-752-36 Uppsala, Sweden
[d] Institute of Geological Sciences, University of Wrocław, Pl. Maksa Borna 9, 50-204 Wrocław, Poland
[e] Department of Geosciences, University of Tübingen, Schnarrenbergstrasse. 94-96, 72076 Tübingen, Germany
[f] Nanochemistry Research Institute, Curtin University, PO Box U1987, WA, 6845 Perth, Australia

ARTICLE INFO

Editor Name: Dr. Oleg Pokrovsky

Keywords:
Lead carbonate
Lead apatite
Dissolution-precipitation
Mineral replacement
Water remediation
Arsenic

ABSTRACT

Water pollution by arsenic is a growing concern due to its toxicity and health effects, prompting research on its immobilization. A novel method for removing arsenate ions from water using synthetic or natural cerussite powder ($PbCO_3$) is proposed. Laboratory experiments over three months at pH 2–8 show that in the presence of chloride ions, cerussite transforms into $Pb(AsO_4)_3Cl$ (mimetite), and in their absence, into $Pb(AsO_4)_3OH$.

Arsenate is removed as lead carbonate dissolves and mimetite precipitates, achieving a removal efficiency of 57–99.9 %. Repeated treatments can enhance this efficiency to over 99 %, with the cerussite powder being reusable. Atomic Force Microscopy experiments show that mimetite formation is surface-controlled, and cerussite reacts with arsenate through a dissolution-precipitation mechanism, partially armouring the cerussite surface.

Repeating the experiments with cerussite in the presence of other cations (Mn, Fe, Ni, Cu, Zn, Cd, Al) or anions (CO_3^{2-}, SO_4^{2-}, PO_4^{3-}, F^-) showed that their presence has no significant effect on the progress and efficiency of the process. Only Al may slightly reduce the effectiveness. Reaction with solutions with an initial concentration of 5 mg As/L resulted in a 99.9 % reduction in As content. Similar observations were noted in experiments using natural arsenic-enriched waters (~0.1 mg As/L), though the reaction proceeded more slowly, requiring additional time for arsenate removal to reach completion. These findings suggest that cerussite removes arsenate from water by gradually being replaced with mimetite crystals. While challenges remain in optimizing this method, it has the potential to become a novel technology for arsenic-contaminated water remediation.

1. Introduction

Arsenic, ranked among the most toxic elements, is classified as the first most toxic substance in the US Toxic Substances and Disease Registry, followed by lead and mercury (ATSDR, 2024). Arsenic forms numerous minerals—over 245 identified types—and is mobilized in the environment through natural processes such as weathering, biological activity, geothermal events, and volcanic eruptions, as well as by human actions that contribute to its spread and distribution (Cheng et al., 2009; Murcott, 2012; Migaszewski et al., 2018; Alka et al., 2021). This element's mobility and transformation in the environment can be triggered by a range of physical, chemical, and biological processes. Large aquifers in many parts of the world are identified with problems from As occurring above acceptable concentrations, resulting in the fact that 226 million people are exposed to arsenic contamination (Murcott, 2012). The toxicity of As and its impact on human health drives intense research on arsenic removal (Smedley and Kinniburgh, 2002; Banning, 2021).

Human activities significantly influence its mobility and distribution in the environment. It is commonly found in acid mine drainage (AMD) and mining waste sites, where sulfide-rich waste materials, left from historic mining activities, can undergo oxidation. This process generates

* Corresponding author.
E-mail addresses: estepien@agh.edu.pl (E. Stępień), mjulia@uni-muenster.de (M. Julia), daniel.buczko@geo.uu.se (D. Buczko), martina.bottaro@uni-tuebingen.de (M. Bottaro), andreas.kappler@uni-tuebingen.de (A. Kappler), gpmmanec@cyf-kr.edu.pl (M. Manecki), putnisc@uni-muenster.de (C.V. Putnis).

https://doi.org/10.1016/j.chemgeo.2024.122531
Received 6 August 2024; Received in revised form 12 November 2024; Accepted 29 November 2024
Available online 6 December 2024

AMD, characterized by low pH (often <4) and high concentrations of dissolved toxic metals and metalloids, including arsenic, lead, cadmium, copper, and zinc (Cheng et al., 2009; Romero et al., 2010). Arsenic concentrations in AMD are highly variable, ranging from below detection limits to values as high as 340,000 μg/L in mine drainage across the U.S. (Plumlee et al., 1997). The maximum recorded arsenic concentration in AMD, 850,000 μg/L, was detected in an acid seep at Iron Mountain, California (Nordstrom and Alpers, 1999). For comparison, arsenic levels in natural water bodies generally vary between <0.5 μg/L and >5000 μg/L, with most freshwater systems containing <10 μg/L (Smedley and Kinniburgh, 2002).

Arsenic exists in various oxidation states, including −3, 0, +3, and +5, but in aquatic environments, arsenic occurs primarily as inorganic oxyanions, arsenite (As(III)) and arsenate (As(V)), with the specific species determined by redox conditions and pH. Organic arsenic compounds can be generated through biological processes, particularly in surface waters, although they generally do not play a significant quantitative role. However, these organic forms may be more prevalent in areas significantly affected by industrial pollution (Smedley and Kinniburgh, 2002.

As(III) species, generally found as H_3AsO_3 or $H_2AsO_3^-$ in more reduced, anoxic environments, are highly toxic and mobile. As(V), commonly present as $H_2AsO_4^-$ and $HAsO_4^{2-}$ in oxidizing environments like acid mine drainage (AMD), is comparatively less toxic and more strongly adsorbed onto mineral surfaces. Both species can exist simultaneously in AMD, where their relative abundance is shaped by oxygen exposure, redox conditions, and interactions with arsenic-oxidizing bacteria. In many AMD sites, arsenate dominates due to prolonged exposure to oxygen and ferric iron, which promotes oxidation from As (III) to As(V) (Smedley and Kinniburgh, 2002; Paikaray, 2015). The focus of this study is on As(V) removal, particularly relevant for AMD and oxidized environments where arsenate dominates.

Arsenic immobilization in the environment occurs through natural processes of precipitation of low-solubility salts and adsorption on soils and sediments. Technologies to remediate arsenic polluted waters follow the same principles, and the most commonly used techniques are based on phenomena of precipitation, adsorption and ion exchange (Sorg and Logsdon, 1978; Pierce and Moore, 1982; Kartinen Jr and Martin, 1995; Driehaus et al., 1995; Manning and Goldberg, 1997; Bothe and Brown, 1999; Magalhães, 2002; Mohan and Pittman, 2007; Nicomel et al., 2015; Mohanty, 2017; Putnis and Putnis, 2022). The remediation strategy explored in this research involves using cerussite ($PbCO_3$) to precipitate arsenate as mimetite ($Pb_5(AsO_4)_3Cl$), inspired by previous work showing the formation of poorly soluble pyromorphite ($Pb_5(PO_4)_3Cl$) from lead-contaminated solutions (Wang et al., 2013; Kwaśniak-Kominek, 2018; Manecki et al., 2020). Pyromorphite and its arsenate analogue mimetite are part of the apatite supergroup and are characterized by low solubility and high stability (Gołębiowska et al., 2002; Bajda, 2010; Flis et al., 2011; Hughes and Rakovan, 2015; Turek et al., 2015; Bajda et al., 2019). Their formation in remediation contexts offers a promising pathway for Pb or As immobilization, as they are highly stable and remove contaminants effectively through precipitation (Ma et al., 1994, 1995; Xu and Schwartz, 1994; Cotter-Howells and Capron, 1996; Laperche et al., 1997; Manecki et al., 2000; Manecki, 2019). We present laboratory findings that evaluate the efficiency of arsenate removal through mimetite precipitation. Observations highlight the mineralogical transformations occurring during the cerussite-arsenate interaction, including pseudomorphic replacement by interface-coupled dissolution-precipitation (ICDP) (Putnis, 2002, 2009; Putnis and Putnis, 2007; Kasioptas et al., 2011; Putnis and Ruiz-Agudo, 2013; Ruiz-Agudo et al., 2014; Wang et al., 2013; Manecki et al., 2020). The proposed method leverages these mechanisms to provide a potential low-cost, effective solution for the treatment of arsenate-contaminated waters, especially in environments affected by AMD or industrial discharges. Laboratory solutions designed to mimic contaminated waters, as well as natural waters from springs enriched in arsenic, were utilized in the experiments.

Results of the study may also shed light on the behaviour of arsenic in the specific rare environments such as oxidized polymetallic hydrothermal ores, milltailings or environments polluted by arsenic pesticides. The formation of arsenates in similar environments can significantly influence the dissolved concentrations of both arsenic and the specific metal involved. Among the numerous secondary arsenate minerals containing zinc, copper, lead, nickel, and cobalt, several may be prevalent and play a crucial role in regulating the dissolved concentrations of arsenic in specific natural settings (Magalhães and Silva, 2003; Drahota and Filippi, 2009).

2. Materials and methods

2.1. Materials

A summary of the experimental design is presented in Table SM1 (Supplementary Materials). Batch experiments were conducted in open air, using glass laboratory beakers or polyethylene test tubes at 25 °C. Experiments I and III were performed as single trials, while Experiment II was conducted in triplicate. All experiments were carried out in the presence of chloride ions (20 mg/L). However, Experiments I and III were also performed in the absence of Cl^- ions, following the same procedures. This design allowed for a direct comparison of the effects of chloride deficiency on the products and crystallization mechanisms.

All solutions used in the experiments were prepared using double distilled water and analytical grade chemicals (Thermo Scientific Inc. and Chempur Inc.). Sodium arsenate dibasic heptahydrate $Na_2HAsO_4{\cdot}7H_2O$ was used as a source of arsenate ions and sodium chloride NaCl as a source of chloride ions. As a source of Al, Cd, Cu, Mn, Ni and Zn nitrate salts were used. Fe(II) was added in the form of $FeCl_2{*}4H_2O$ (the nitrate salt could not be obtained). Sodium salts were used to supply the chosen anions (SO_4^{2-}, CO_3^{2-}, F^-, PO_4^{3-}). The pH was adjusted using 0.5 M HNO_3 or 1 M NaOH, added dropwise with a pipette, and pH measurements were performed using a pH - meter ELMETRON CPC-401.

Sampling of natural waters was conducted in May 2024. A few litres of waters were collected in Germany, from the technical facility in Vital Therme (Bad Wildbad) and thermal spring (Kochbrunnen Quelle) in Wiesbaden. The water samples were on-site filtered through 0.2- μm pore-sized syringe filters and placed in 50 mL polypropylene tubes (acidified with 2 % HNO_3). In addition, unfiltered water samples were collected and placed in polypropylene bottles. During sample collection, transport, storage and preparation, measures of precaution were taken to reduce the possibility of contamination. Chemical analysis of waters composition is available in supplementary materials (SM, Table 2).

In this study, we use the term 'arsenate' as a general term to refer to all species of As(V) present across the range of pH values studied, including $H_3AsO_4^0$, $H_2AsO_4^-$, $HAsO_4^{2-}$, AsO_4^{3-} These species coexist in dynamic equilibrium, shifting with pH according to established acid-base equilibria. It is important to note that multiple As(V) species may be present across the studied pH range. For simplicity, we refer to 'arsenate' as the species involved in mimetite precipitation, where As(V) reacts with Pb^{2+} and Cl^- to form $Pb_5(AsO_4)_3Cl$.

2.1.1. Synthesis of cerussite

Cerussite crystallized by dropwise mixing of 1900 ml 3.3 % $Pb(NO_3)_2$ solution with 5.25 % $(NH_4)_2CO_3$ was aged for 24 h, centrifuged, washed and dried at 70 °C. No impurities were detected by X-ray diffraction (XRD) or scanning electron microscopy (SEM/EDS) analysis of the homogenous, crystalline precipitate composed of identical needle-like crystals 5 μm in size (SM, Fig. 1).

2.1.2. Experiment I – Removal of As by precipitation of mimetite

To quantify the removal of arsenate by reaction with synthetic cerussite, 0.5 g of synthetic $PbCO_3$ was mixed with 500 mL of solution containing AsO_4^{3-} and Cl^- ions ([As] 50 mg/L, [Cl] 20 mg/L) at pH 2, 4,

6, and 8. The suspension was sampled every two days for one week, with approximately 5 mL of solution and a small amount of solids collected simultaneously using a pipette. The solids were centrifuged (4500 rpm), washed three times with water and air dried.

Given the high efficiency of arsenate removal and the limited release of lead observed during initial reactions, pH 4 was selected for the experiment to investigate cerussite's effectiveness in promoting arsenate sequestration via mimetite precipitation. To monitor any potential decrease in efficiency over repeated use, the experiment at pH 4 was conducted over five consecutive cycles, with each cycle consisting of a 30-min reaction using 0.5 g of the same cerussite powder and 50 mL of fresh arsenate solution. This approach allowed for an assessment of both the stability of cerussite's performance in removing arsenate and its sustained capacity to facilitate mimetite formation under acidic conditions. To evaluate the potential increase in AsO_4 removal efficiency, the experiment was conducted three additional times at pH 4, each with a fresh 0.5 g portion of cerussite but using the solution obtained from the previous run.

2.1.3. Experiment II – Imitating the natural environment

Experiments were conducted on the reaction of cerussite (0.5 g) with arsenate solutions at concentrations of 1, 5, and 10 mg As/L (50 mL of solution, pH 4) to evaluate the effectiveness of arsenic sequestration at lower concentrations typically found in arsenic-contaminated waters.

To simulate natural environmental conditions, commonly present cations (Al, Cd, Cu, Fe, Mn, Ni, Zn) and anions (SO_4^{2-}, CO_3^{2-}, F^-, PO_4^{3-}) were added to solutions containing AsO_4. Then, 0.5 g of $PbCO_3$ was reacted with 50 mL of this solution (pH 4) at initial arsenic concentrations of 5 mg/L or 10 mg/L for up to 24 h. Cations concentrations matched those of arsenic, with both set to 5 mg/L or 10 mg/L, depending on the initial arsenic concentration. The concentrations of SO_4^{2-}, CO_3^{2-}, F^-, PO_4^{3-} were also adjusted according to the arsenic level being tested. When the arsenic concentration was 5 mg/L, SO_4^{2-} and CO_3^{2-} were set at 50 mg/L, and F^- and PO_4^{3-} at 1 mg/L. At an arsenic concentration of 10 mg/L, SO_4^{2-} and CO_3^{2-} were increased to 200 mg/L, and F^- and PO_4^{3-} to 10 mg/L. While these concentrations were chosen arbitrarily, they represent levels that can still be found in contaminated environments, such as those impacted by agricultural runoff or industrial discharges. Experiments were also conducted at higher arsenic concentrations reflective of those commonly found in acid mine drainage, specifically at 50 mg/L of As. In these experiments, the concentrations of cations were set to match the arsenic concentration or doubled (50 or 100 mg/L), while the concentrations of SO_4^{2-} and CO_3^{2-} were set between 500 and 1000 mg/L. Additionally, PO_4^{3-} and F^- concentrations were adjusted to either 5 or 10 mg/L. This setup aimed to replicate conditions typical of contaminated environments, allowing for an evaluation of the reaction efficiency under more extreme scenarios and simulating the complex geochemistry of acid mine drainage systems. The experiments were also conducted by adding each cation and anion separately to the AsO_4 solution to test their individual effects on arsenic sequestration. For these trials, the same initial arsenic concentrations of 5 or 50 mg/L were maintained, with a pH of 4. Each relevant cation (Al, Cd, Cu, Fe, Mn, Ni, Zn) and anion (SO_4^{2-}, CO_3^{2-}, F^-, PO_4^{3-}) was added separately to the AsO_4 solution to assess their individual impacts. This approach allowed for a clearer understanding of how each specific ion interacted with arsenate under controlled conditions. Experiments were also carried out with natural thermal waters sampled in Bad-Wildbad (Vital Therme, Germany; pH 7.59) and Wiesbaden (Kochbrunnen Quelle, Germany; pH 6.70), containing respectively 0.08 and 0.10 mg As/l, at their natural pH.

In these experiments, the suspensions were shaken for one hour and sampled. Approximately 5 mL of the solution was sampled, and after shaking for an additional 24 h, the suspensions were sampled again. The solutions were filtered through 0.2-μm syringe filters and analysed for arsenic and lead concentrations. Solids were sampled after one week using a pipette, washed three times with water and centrifuged (4500 rpm). After that they were air dried and examined using SEM - EDS. A summary of the concentrations and ions used in these experiments is provided in Tables 1–4.

2.1.4. Experiment III - Crystallization mechanisms

To determine the crystallization mechanisms, fragments of natural, optically clear cerussite crystals (Mibladen, Morocco; SM, Table 3) approximately 2–3 mm in size, were reacted with arsenate solution (50 mg As/L) at pH 2, 4, 6 and 8, for up to 1 month. Solids were sampled after one week and after one month, and examined using SEM and EMP WDS. To observe the solid-liquid interface in real time during the nucleation and growth of lead arsenate, we utilized an Atomic Force Microscope (AFM) equipped with a fluid cell (Bruker, Multimode). A fresh, clean cleavage surface of cerussite was prepared and continuously imaged while immersed in an arsenate solution. This setup allowed us to capture high-resolution images over several hours, providing insight into the dynamic processes occurring at the mineral-solution interface during lead arsenate formation. For each experiment acidified water (pH 4) was flowed at a 2 mL/scan rate for 10 min over the sample surface in order to provide a clean surface and was followed by an arsenate solution ([As] 0.16 or 0.5 mM). This flow rate was chosen to confirm a surface-controlled reaction versus a diffusion-controlled (Ruiz-Agudo et al., 2010; Wang et al., 2013). After 10 min of arsenate solution flow, the samples were left in static solution and imaged after 30 min, 1 h, 2 h and after about 20 h in order to observe the longer- term effect of the solutions on the sample surfaces.

2.2. Methods

The concentration of As(V) in solution was determined by the molybdenum blue method (Lenoble et al., 2003) using a HITACHI U-1800 UV–Vis Spectrophotometer at 870 nm (detection limit of 20 μg As(V)/dm^3). Concentrations of Pb were measured using atomic absorption spectrometry (AAS, Savant AA spectrometer, GBC Scientific Equipment) with a detection limit of 0.05 mg Pb/dm^3 at $\lambda = 217$ nm. In the experiments designed to simulate natural environmental conditions, concentrations of As and Pb in the solutions were quantified by inductively coupled plasma mass spectrometry (ICP - MS, Agilent 7900). Samples for ICP measurements were diluted with 2 % (*v*/v) analytical grade HNO_3.

Conventional X-ray powder diffraction patterns were obtained on samples ground in agate mortar using Rigaku SmartLab diffractometer (2-72° 2θ, 0.02° step size, 1 s/step). The phases were identified using the PDF-2 JCPDS data base and XRAYAN software (Marciniak et al., 2006). FEI Quanta 200FEG Scanning Electron Microscope (SEM) equipped with an Energy Dispersive Spectroscopy (EDS) was used to characterize the morphology and elemental composition of the solids. Air-dried powders were mounted on double-stick tape and imaged in low vacuum with no coating.

Substrates and products of the experiments were also analysed (point Wavelength-Dispersive Spectroscopy WDS analysis, element distribution mapping) using Field Emission-Electron Probe Micro-Analyser (FE-EPMA; JEOL JXA8530F Superprobe) at the National Electron Microprobe Laboratory at the Department of Earth Sciences, Uppsala University, Sweden. Natural crystals were epoxy-mounted, sectioned, polished, and carbon-coated in preparation for the analysis. Cerussite and mimetite point analyses were conducted at acceleration voltage of 15 kV, with probe current of 10 nA and 20 nA respectively (analytical spot size of 1 μm maximum). A real distribution of elements was mapped using identical acceleration voltage at increased probe current (40 nA) with resolution (step) of 0.5 μm × 0.5 μm and dwell time of 100 ms.

In situ dissolution experiments were performed using a Digital Instruments (Bruker) Nanoscope Multimod AFM working in contact mode and equipped with an O-ring sealed fluid cell (Institut für Mineralogie, University of Münster, Germany). Si_3N_4 tips (Nunano SCOUT 70 RAu tips) with spring constants of 2 N/m were used for imaging in solution. AFM images were analysed using the NanoScope software (Version

5.31r1) and WSxM v5.0 Develop 6.4 (Horcas et al., 2007; Wang et al., 2013).

3. Results and discussion

3.1. Experiment I – Removal of As by precipitation of mimetite

The reaction of cerussite with arsenate solution resulted in removal of As from solution. The most significant decrease in arsenate concentration occurred during the first 24 h (Fig. 1). The efficiency of removal decreased with an increase in pH from 94 % at pH 2 to 60 % at pH 8. After 7 days of the reaction, a decrease of arsenate concentration from 50 mg to values less than 2.76 mg As/L was observed, and the final efficiency of its removal was comparable throughout the pH range.

Multiple treatments did not exhaust the potential of cerussite to remove arsenate and form mimetite. The reaction of synthetic cerussite with a solution containing AsO_4 was repeated 5 times at pH 4 with a fresh solution but using the solids from the previous run. Only after a third run a slight decrease in the removal efficiency was observed; after a fifth run the efficiency decreased from over 99 % to about 96 %. The highest efficiency of 99.9 % of arsenate sequestration was obtained by reacting the same solution three times successively with fresh portions of cerussite.

The concentration of Pb^{2+} present in the solution after 7 days of reaction of cerussite with arsenate solution ranged from 58.6 mg Pb/L at pH 2 to 0.1 mg Pb/L at pH 8. In a neutral and alkaline system lead carbonate dissolved more slowly as expected from a carbonate mineral (Pokrovsky and Schott, 2002). A summary of the concentrations of As and Pb in the solutions after the experiments is presented in Table 4, SM.

Although arsenate removal was initially less efficient at pH levels of 4 to 8 compared to pH 2, by the end of the 7-day reaction period, the overall arsenate uptake was comparable across the different pH levels. However, the Pb concentrations at pH 2 far exceeded the drinking water standard (10 μg Pb/L), indicating significant mobilization of lead, a highly toxic trace metal. The levels at pH 4 to 8, while still elevated, were markedly lower, making these pH conditions more favourable for potential applications. To further mitigate lead release from the solution, a promising approach would involve utilizing phosphates, which has been previously studied and patented for their ability to precipitate crystalline lead chlorophosphate – pyromorphite $Pb_5(PO_4)_3Cl$, effectively removing lead from the solution (Ma et al., 1994, 1995; Xu and Schwartz, 1994; Cotter-Howells and Capron, 1996; Laperche et al., 1997; Manecki et al., 2000; Manecki, 2019). This dual approach—efficient arsenate removal at a higher pH while minimizing lead mobilization—highlights the importance of optimizing reaction conditions to enhance the safety and efficacy of this treatment method.

Crystallization of mimetite occurred as a result of the dissolution of cerussite releasing Pb^{2+} into a mineral-fluid boundary layer, followed by reaction with AsO_4^{3-} and Cl^- ions present in solution:

dissolution of cerussite: $PbCO_3 \Rightarrow Pb^{2+} + CO_3^{2-}$

precipitation of mimetite: $5Pb^{2+} + 3AsO_4^{3-} + Cl \Rightarrow Pb_5(AsO_4)_3Cl\downarrow$

The extremely low solubility of mimetite ensured that, at equilibrium, both arsenic and lead concentrations remained minimal. This resulted in significantly lower lead levels than those that would be present if cerussite dissolved in pure water (Fig. 2, SM). The above reactions can be simulated using PHREEQC (Parkhurst and Appelo, 1999). Details of the model reactions are presented in the supplementary material (Table 5A, SM). Large discrepancies were observed in the concentrations predicted by the model and measured experimentally (Table 6, SM). The main reason for the discrepancy was probably the failure to reach equilibrium at experimental conditions. In the modelling efforts, solubility constants derived from the PHREEQC database were utilized; however, we acknowledge that the accuracy of these values, particularly for mimetite, can vary significantly. The reported solubility products for mimetite are influenced by experimental conditions, such as temperature and ionic strength. Additionally, the presence of competing ions may further complicate the solubility dynamics of lead and arsenate phases (Stumm and Morgan, 2013). Due to limitations in existing thermodynamic data and the variability in solubility constants reported in different studies (e.g. Voigt et al., 2018; Sahai and Schoonen, 2020; Lu et al., 2022), it is challenging to precisely quantify the source of discrepancy between our experimental and modeled values. Nevertheless, the model confirmed that the efficiency was strongly dependent on pH. It allowed predicting, in agreement with the experimental results, that although theoretically the lowest final As concentrations can be achieved at pH 2, this is accompanied by a potentially very high concentration of unwanted excess Pb released. Both computer modelling and experimental results at different pH values indicated that the optimal pH range for the application of arsenate removal method was 4–6.

The reaction effectiveness depended on the pH, but in all cases the product was mimetite (Fig. 3, SM). Precipitation of mimetite incrustations on the surface of cerussite crystals was observed already after 1 h of the reaction with arsenate solutions within the whole pH range, with the amount of mimetite increasing over time. At pH 2,

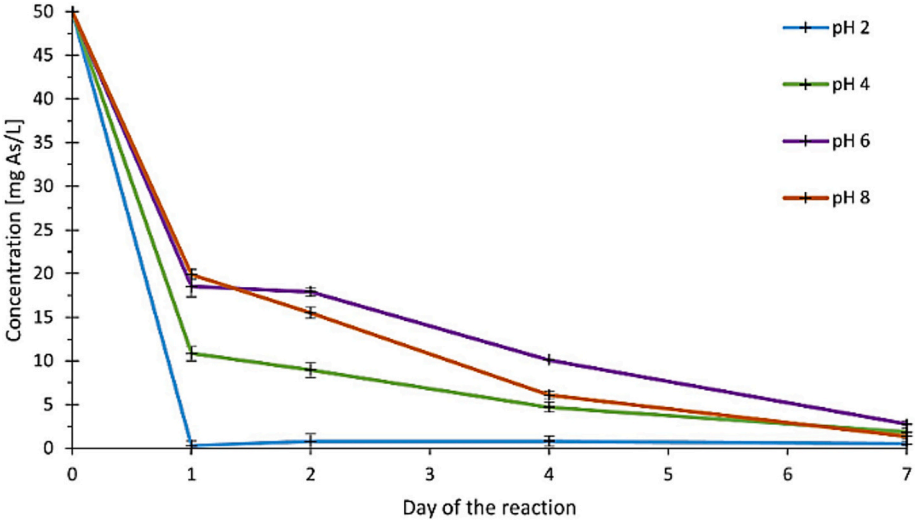

Fig. 1. Decrease in arsenate concentration over time at various initial pH values resulting from the reaction of a solution containing 50 mg As/L with cerussite powder for 7 days.

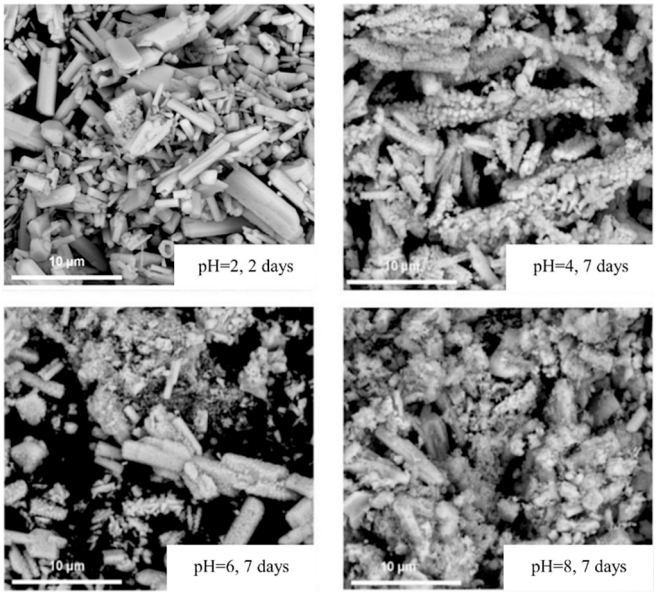

Fig. 2. Products of cerussite reaction with solution containing 50 mg As/L. SEM images in backscattered electrons mode (BSE).

initially both heterogeneous and homogeneous precipitation was observed (Fig. 2). As the reaction proceeded, cerussite dissolved completely at the conditions of the experiment. Mimetite crystals recrystallized by Ostwald ripening into larger, hexagonal, euhedral rods. At higher pH cerussite did not dissolve completely. Also, the higher the pH, the finer the mimetite crystals in the form of euhedral to subhedral hexagonal rods, approximately 2.5 µm in size. They formed two morphological populations: thick and thin rods. At pH 4–8, mimetite precipitated as hexagonal needles less than 1 µm in size. The variation in size and morphology of Pb-apatites synthesized by precipitation in aqueous solutions under different conditions was reported by Sordyl et al. (2022). The shape and size of the precipitate crystals were a function of concentration, pH and mixing parameters.

3.2. Experiment II – Imitating the natural environment

In the experiments conducted in the absence of other cations and anions, with only arsenate and chloride present, at much lower arsenic concentrations (1 to 10 mg/L) compared to the experiments where 50 mg As/L was used, after 1 h the decrease of arsenate in solution reached 98.0 to 99.7 % (Table 1). The maximum decrease (99.7 %) was observed at an initial concentration of [As] = 10 mg/L, while the lowest (98.0 %) occurred at a concentration of 1 mg As/L. This suggests that cerussite is particularly effective at low arsenate levels, which are more typical in environmental contamination scenarios. The near-complete reduction efficiency observed throughout this concentration range indicates that the method could be suitable across the entire range, underscoring cerussite's potential applicability in settings where arsenate contamination falls within these levels.

Added cations except aluminium did not reduce the sequestration efficiency of arsenate. At low As (5 mg/L) and cations (5 or 10 mg/L) initial concentrations, arsenate removal efficiency after 1 h was in the range of 85.0 to 99.9 % (Table 2). Reaction carried out at high initial arsenic (50 mg /L) and high cations concentrations (50 to 100 mg/L) resulted in lower As sequestration (between 46.6 and 99.8 %) (Table 3). For both low and high initial concentrations of As, the lowest (%) arsenate sequestration efficiency was observed in the presence of aluminium, both at low (5 mg As/L) and high (50 mg As/L) initial concentrations.

Table 1
Final concentrations of As and percent efficiency in As removal resulting from the experiments at low initial arsenate concentrations, in the absence of accompanying ions.

Initial As concentration [mg/L]	Concentration of As after 1 h [mg/L]	As removal efficiency [%]
1	0.02	98.0
5	0.06	98.8
10	0.03	99.7

Low concentrations of anions added to the solutions had no significant effect on the removal of arsenate from the aqueous solution, and arsenate sequestration efficiency ranged from 98.4 to 99.8 % (Table 3). When the initial As level was 50 mg/L, in the presence of anions, arsenate sequestration reached from 83.4 to 99.9 % (Table 4). Only the addition of SO_4^{2-} anions affected the amount of immobilized arsenate, but the decrease in efficiency was not related to the increase in its level in solution.

When cations and anions were present together in one solution at both low and higher concentrations, almost complete sequestration of arsenate occurred (99.5 % to 99.6 %) (Table 5). This finding highlights mimetite's high selectivity for arsenate in complex matrices, suggesting that ions do not significantly hinder the overall removal process. The experiment conducted with natural waters showed that the arsenate removal reaction proceeds, but at a slower rate compared to the higher arsenic concentrations used in experiments simulating natural solutions mentioned above. In the first hour of the reaction, approximately 7 % of arsenic is removed from the Bad Wildbad water, while 17 % is removed from the Wiesbaden water. After 7 days, arsenic sequestration reaches 37.1 % in the Wiesbaden water and 73.8 % in the Bad Wildbad water (Table 5). These tests have shown that arsenate reduction is much slower for "natural systems", probably due to its lower initial concentrations, complex water chemistry or reduced reaction kinetics. Cerussite could perform effectively under certain natural conditions, however additional experiments with a broader range of water types is needed to assess its effectiveness in diverse environmental scenarios, and longer reaction times may be necessary for complete removal.

Mimetite was detected by SEM-EDS analysis in all sediments after the reaction of cerussite with solutions containing high ion concentrations. Identifying mimetite crystallization in precipitates formed from reactions at low arsenic concentrations was challenging due to the very small amount of precipitate. However, repeated reactions using the same cerussite powder, each time with a fresh solution containing arsenic and accompanying ions, allowed for confirmation of mimetite formation (Fig. 3A and B; Fig. SM4A). In all cases it precipitated heterogeneously in a form of incrustations on the surface of dissolving cerussite. Sometimes, also homogenous rods of mimetite were observed among cerussite crystals (Fig. 3A and B). No other mineral phases were observed in the SEM analysis of the cation interactions. In contrast, when cerussite and anions were both present, it led to the precipitation of lead sulphate ($PbSO_4$) (Fig. 3C and Fig. SM4B) and a phosphate-arsenate solid solution (Fig. 3D and Fig. SM4C). This suggests that the presence of anions significantly influenced the mineralogy of the system by promoting the formation of specific other lead compounds.

The tendency of 'apatite-like' solids, including mimetite, to incorporate various metal ions into their crystal lattice suggests that the immobilization of arsenate by mimetite could be influenced by the presence of other dissolved metal ions (Ma et al., 1994b). Herein, the introduction of additional cations like Cd, Cu, Fe(II), Mn, Ni and Zn at both low and high arsenic concentrations did not interfere with arsenate removal. However, aluminium consistently lowered arsenate removal. The observed decrease in arsenate removal in the presence of Al likely stems from its unique behaviour in aqueous environments, particularly at acidic to neutral pH. Aluminium ions can hydrolyse to form various hydroxyl species (such as $[Al(OH)]^{2+}$ and $[Al(OH)_2]^{+}$), which can interfere with the surface chemistry of cerussite by altering its charge or creating a competitive binding layer on the surface (e.g. Dzombak and

Table 2
Final concentrations of As and percent efficiency in As removal resulting from the experiments in the presence of accompanying cations at low initial concentrations.

Initial As concentration = 5 mg/L							
Assumed ratio of As to metal 1:1	Accompanying element						
	Al	Cd	Cu	Fe	Mn	Ni	Zn
Arsenic concentration after 1 h of reaction [mg/L]	0.110	0.070	0.020	0.020	0.010	0.060	0.020
Arsenate sequestration efficiency [%]	97.8	98.6	99.6	99.6	99.9	98.8	99.6
Assumed ratio of As to metal 1:2	Accompanying element						
	Al	Cd	Cu	Fe	Mn	Ni	Zn
Arsenic concentration after 1 h of reaction [mg/L]	0.750	0.010	0.030	0.080	0.090	0.060	0.030
Arsenate sequestration efficiency [%]	85.0	99.3	99.8	99.8	99.1	99.4	99.8

Table 3
Final concentrations of As and percent efficiency in As removal resulting from the experiments in the presence of accompanying cations at high initial concentrations.

Initial As concentration = 50 mg/L							
Assumed ratio of As to metal 1:1	**Accompanying element**						
	Al	**Cd**	**Cu**	**Fe**	**Mn**	**Ni**	**Zn**
Arsenic concentration after 1 h of reaction [mg/L]	13.965	0.023	0.020	0.002	0.004	0.001	0.009
Arsenic sequestration efficiency [%]	74.7	99.9	99.9	99.9	99.9	99.9	99.9
Assumed ratio of As to metal 1:2	**Accompanying element**						
	Al	**Cd**	**Cu**	**Fe**	**Mn**	**Ni**	**Zn**
Arsenic concentration after 1 h of reaction [mg/L]	30.747	0.006	0.020	0.003	0.002	0.003	0.006
Arsenic sequestration efficiency [%]	46.6	99.9	99.9	99.9	99.99	99.9	99.9

Table 4
Table. Final concentrations of As and percent efficiency of its sequestration resulting from the experiments in the presence of accompanying anions.

Anion	Initial anion concentration [mg/L]	As concentration after 1 h of reaction [mg/L]	As sequestration efficiency [%]
	Initial As concentration 5 mg/L		
SO_4^{2-}	50	0.000	99.9
	100	0.020	99.6
	200	0.010	99.8
CO_3^{2-}	50	0.030	99.4
	100	0.020	99.6
	200	0.050	99.0
PO_4^{3-}	5	0.030	99.4
	10	0.030	99.4
F^-	5	0.080	98.4
	10	0.020	99.6
	Initial As concentration 50 mg/L		
SO_4^{2-}	250	0.040	99.9
	500	8.936	83.4
	1000	0.041	99.9
CO_3^{2-}	250	0.050	99.9
	500	0.053	99.9
	1000	0.054	99.9
PO_4^{3-}	5	1.469	97.2
	10	0.789	98.6
F^-	5	1.014	98.2
	10	0.006	99.9

Table 5
Final concentrations of As and percent efficiency of its sequestration resulting from the experiments in the presence of the mixture of accompanying cations and anions or natural waters.

Initial As concentration = 5 mg/L		
Accompanying ions	As concentration after 1 h of reaction [mg/L]	As sequestration efficiency [%]
Al, Cd, Cu, Fe(II), Mn, Ni, Zn = 5 mg/L PO_4^{3-}, F^- = 1 mg/L CO_3^{2-}, SO_4^{2-} = 50 mg/L	0.020	99.6
Al, Cd, Cu, Fe(II), Mn, Ni, Zn = 10 mg/L PO_4^{3-}, F^- = 10 mg/L CO_3^{2-}, SO_4^{2-} = 200 mg/L	0.030	99.4
Initial As concentration = 50 mg/L		
Accompanying ions	As concentration after 1 h of reaction [mg/L]	As sequestration efficiency [%]
Al, Cd, Cu, Fe(II), Mn, Ni, Zn = 50 mg/L PO_4^{3-}, F^- = 5 mg/L CO_3^{2-}, SO_4^{2-} = 500 mg/L	0.099	99.7
Al, Cd, Cu, Fe(II), Mn, Ni, Zn = 100 mg/L PO_4^{3-}, F^- = 10 mg/L CO_3^{2-}, SO_4^{2-} = 1000 mg/L	0.031	99.9
Natural As-enriched waters		
Water sampling location and As concentration	As concentration after 24 h of reaction [mg/L]	As sequestration efficiency [%]
Wiesbaden, Kochbrunnen Quelle, Germany 0.10 mg As/L	0.064	37.1
Bad Wildbad, Vital Therme, Germany 0.08 mg As/L	0.022	73.8

Morel, 1991; Brown et al., 1985). This interaction might prevented arsenate ions from accessing active binding sites or disrupted the formation of stable lead-arsenate compounds.

Other anions that could potentially compete with arsenate, such as PO_4^{3-}, SO_4^{2-}, or CO_3^{2-}, did not significantly interfere with its removal from solution (Ma et al., 1994; Manning and Goldberg, 1996;). Darland and Inskeep, 1997; Lytle et al., 2005; Ghosh et al., 2006; Biswas et al., 2014; Campbell and Nordstrom, 2014). In this case it promoted the formation of solids such as lead phosphate-arsenate. The presence of these two ions can promote co-precipitation, forming solid solutions that stabilize arsenate in the environment. Sulfate (SO_4^{2-}) somewhat reduced the immobilization efficiency at higher concentrations, possibly due to its potential to form competing complexes with lead (lead sulfate

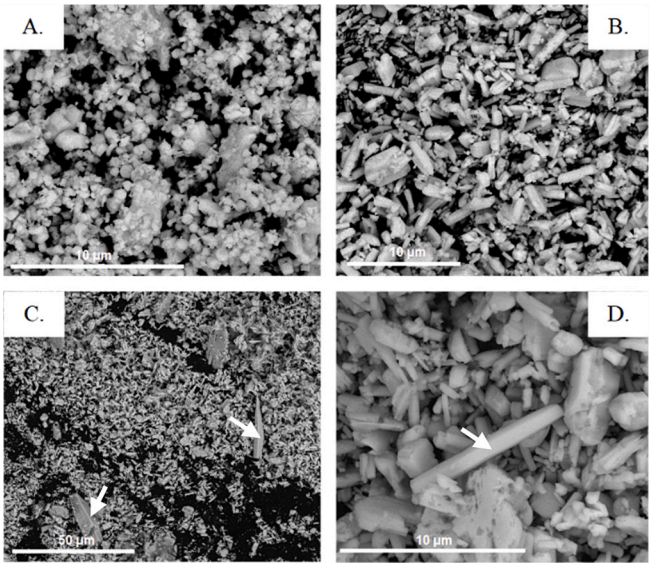

Fig. 3. Products of the cerussite reaction with a solution containing 5 mg As/L and accompanying ions. A and B - the multiple reactions of cerussite with low-concentration arsenate solutions, leading to the formation of mimetite precipitates as heterogenous incrustations, as well as homogenous crystals. C. The precipitation of lead sulfate ($PbSO_4$) in the presence of sulfate ions (SO_4^{2-}) (indicated by arrows). D. The formation of a phosphate-arsenate solid, following the addition of phosphate ions (PO_4^{3-}) to the arsenate-containing solution (indicated by an arrow). All images are captured in backscattered electron mode (BSE) using scanning electron microscopy (SEM).

precipitation), though the lack of a clear correlation suggests a secondary, rather than primary, interference mechanism.

The natural water experiments were simulated using PHREEQC, with detailed reaction models provided in the supplementary material (Table 5B and C, SM). Modelling results indicated that fluoride enrichment in both water samples could influence arsenic speciation and potentially affect mimetite precipitation. Nonetheless, our experimental results showed a decrease in arsenic concentration, suggesting that mimetite formation may proceed despite the presence of fluoride. Modelling at higher concentrations of arsenic (5 mg/L) and fluoride (5 mg/L) indicated that mimetite precipitation is possible under these conditions, a finding supported by experiments with synthetic solutions (Table 2 and 3). This suggests that initial arsenic concentration is a critical factor; at higher levels, supersaturation can be achieved, enabling mimetite precipitation even in the presence of fluoride. These results further indicate that the method we are testing is more suitable for waters with higher arsenic concentrations, such as 5 mg As/L, as mimetite precipitation is hindered at lower arsenic concentrations (e.g., 0.1 mg As/L) in the presence of fluoride.

Modelling results have shown the potential formation of arsenic-fluoride complexes, such as AsO_3F^{2-} and $HAsO_3F^-$, under certain conditions. These complexes indicate that fluoride could influence arsenate speciation beyond simple competitive binding with lead. Fluoride ions, by forming such species, may indirectly impact mimetite formation by reducing free arsenate availability for lead complexation. Additionally, fluoride can affect the solution's pH through interactions with hydrogen ions, which in turn could alter the stability and precipitation conditions for mimetite, which typically favours a pH range of 4–8.

Additionally, aluminium ions may impact arsenate removal through reactions with cerussite. Al ions can directly react with arsenate to form aluminium arsenate phases (e.g., $AlAsO_4$) under appropriate conditions. Aluminium readily undergoes hydrolysis in aqueous solutions, particularly at pH levels above 4, leading to the formation of species such as $Al(OH)_3$ and other hydrolysed forms. These species can interfere with mimetite nucleation by providing alternative sites for crystallization or by precipitating as separate aluminium hydroxide or arsenate phases, potentially reducing the availability of arsenate for lead complexation. Modelling results, supported by experiments with synthetic solutions, indicated that arsenic removal was influenced by the presence of aluminium, with arsenate removal decreasing compared to experiments where aluminium was not present. This further suggests that aluminium can hinder the efficiency of mimetite precipitation in arsenic sequestration.

3.3. *Experiment III– Crystallization mechanisms*

3.3.1. *In-situ AFM experiments*

Observations with AFM indicated that the nucleation process is surface controlled, and mimetite formed initially as nanoparticles (Fig. 4). Dissolution of cerussite began immediately on contact with deionized water (Fig. 5, SM). In the presence of arsenate ions at pH 4, widespread surface etching with step retreat was observed and etch pit steps were filled with precipitating mimetite (verified by SEM/EDS observations after the experiment; Fig. 6, SM). Direct in-situ observations showed the nucleation of mimetite occurred directly on the surface of the cerussite crystal, rather than in the aqueous solution. A clear control of the cerussite surface on the precipitation of mimetite nanoparticles was observed. AFM scans revealed that mimetite particles remained firmly attached to the cerussite surface, resisting removal by the AFM scanning tip. This firm attachment indicates a possible interaction between the cerussite structure and the mimetite nanoparticles at the surface, although the precise nature of this interaction—whether chemical or physical—requires further investigation. That may also be due to the fact that the supersaturation at the mineral - solution interface is higher than in the bulk solution, indicating a possibility of surface-controlled dissolution. However, a quantitative assessment of transport and diffusion rates would be necessary to confirm any diffusional or transport control over the surface reaction. In natural environments, heterogeneous nucleation is recognized as the primary pathway for mineral formation from aqueous solutions (Chernov, 1984; Stumm and Morgan, 1985; Wang and Morse, 1996; Fernandez-Diaz et al., 2009). Similar mechanisms have been documented, such as iron oxyhydroxide precipitation on siderite (Renard et al., 2017) and selenium/arsenic phase formation on calcite (Putnis et al., 2013; Renard et al., 2015).

The reaction between cerussite and arsenate ions has not been previously studied. However, AFM studies have been conducted at the cerussite-phosphate interface (Wang et al., 2013). The results indicated that the cerussite surface was rapidly covered by a layer of precipitating pyromorphite $Pb_5(PO_4)_3Cl$, which effectively passivated the crystal surface. Elongation and/or widening of the needle-like lead phosphate crystals were not observed already after 10 min of the reaction time. The opposite was observed in our experiments. In-situ AFM fluid cell experiments revealed that the cerussite surface was not initially passivated by the mimetite precipitate. In time an increase in the size and height of mimetite aggregates was detected by AFM even after 3 h (Fig. 3 and Fig. 7, SM). Initial small nanoparticles (100–200 nm) merged to form larger particles (300–600 nm). However, in the batch experiments conducted with natural cerussite crystals and AsO_4 solutions after a period of one week to one month of reaction, no further transformation of the parent phase was observed in SEM images. This indicates that the reaction was fast mostly for the first few hours which is consistent with an observed fast decline in the As content in the solution (Experiments I and II).

The shape of the resulting crystals depended on the pH of the experimental solution. During the reaction when the pH is 8, the newly formed Pb-arsenate formed aggregates of crystals with a rounded shape, which over time developed a solid layer of precipitate covering the entire scanned area. In contrast, when the experimental solution was more acidic (pH 4), the precipitate developed in a different way. Aggregates of crystals were observed on the surface of the dissolved cerussite, which did not form a layer covering the area. They nucleated

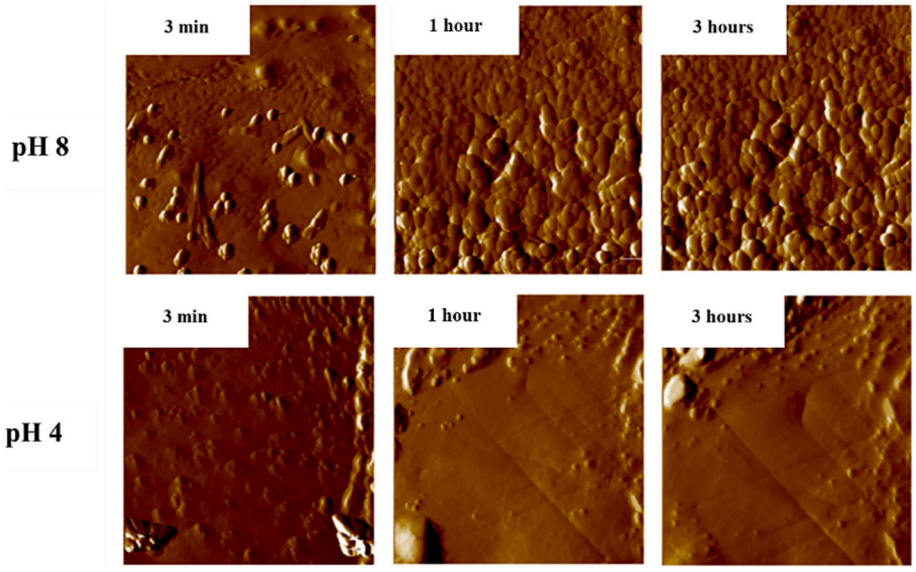

Fig. 4. AFM deflection images illustrating dissolution of cerussite surfaces exposed to an arsenate solution (0.5 mM As/L) at pH 8 and at pH 4. Results show the precipitation of nanoparticles of a new As-rich phase on the cerussite surface. When the pH value was 4, the precipitate was partially dissolved by the AFM scanning process, and some particles were pushed to the margins of the scanned area. Images are 5 × 5 μm.

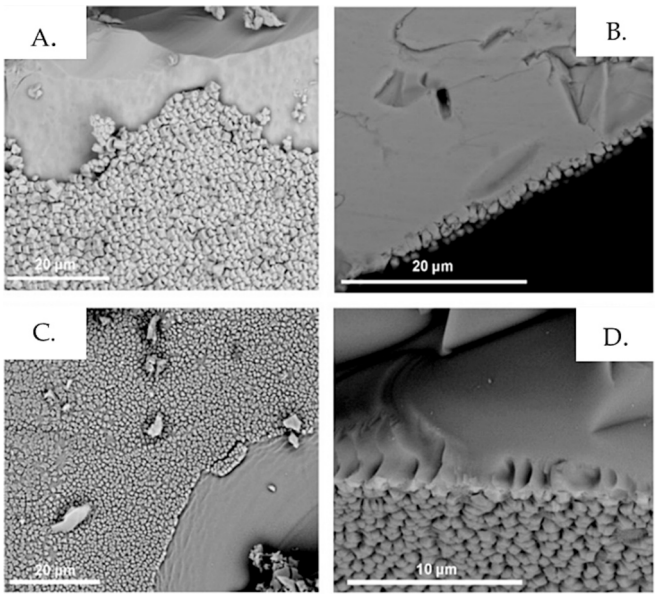

Fig. 5. BSE images of cerussite crystals covered with a mimetite crust(A). The crust is approximately 1 μm thick (B) and falls off easily with a noticeable gap occurring at the reaction front (C). Voids between mimetite crystals allow potential infiltration of fluids through the crust (D).

as rounded or shapeless grains that form a kind of particle "belt", which grows over time. The precipitates had no preferential locations - they were observed both at edge steps and terraces on the surface.

The morphology of Pb-arsenate precipitates depended on the pH of the experimental solution, likely due to pH-dependent changes in mimetite's solubility and precipitation kinetics. According to published solubility data (Bajda, 2010), mimetite exhibits minimal solubility at neutral to slightly alkaline pH (6–8), which promotes the formation of a stable, solid crust across the surface. Under these conditions, Pb-arsenate precipitation was more uniform, resulting in a continuous layer.

In contrast, at acidic pH (4), the solubility of mimetite increased, which likely enhanced localized dissolution, leading to the observed

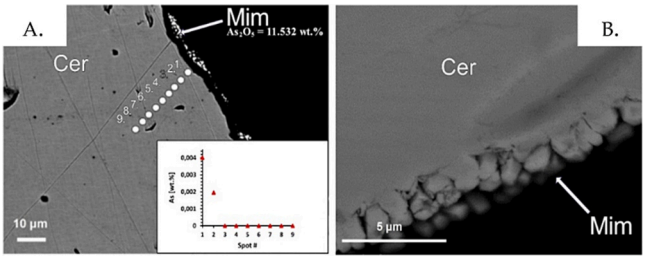

Fig. 6. BSE image of a cut and polished cerussite crystal reacted with arsenate solution and the results of microprobe analysis. The cerussite crystal is not transformed and As does not penetrate underneath the crust (A). A close-up of mimetite crust shows tooth-like crystals attached to cerussite (B).

formation of rounded or shapeless particle aggregates rather than a cohesive crust. This effect was especially pronounced in areas of high lead availability, such as etch pits and step edges, where localized supersaturation enabled particle nucleation and growth. SEM-EDS analysis (Fig. 6, SM) performed after AFM experiments revealed dissolution features of the cerussite crystal that are more significant for the reaction proceeding at pH 4. Pb arsenates precipitated on the cerussite surface appearing as needle-shaped and hexagonal dendritic crystals. The precipitate formed under alkaline conditions developed as a porous, solid crust, but aggregates of single crystals growing directly from the cerussite surface were also observed. In contrast, a cerussite crystal reacted with an arsenate solution at acidic pH was not covered by a crust. In most cases mimetite crystallize in etch pits formed during $PbCO_3$ dissolution. In these areas, the expected release of lead into solution is highest, allowing new crystals to develop easily.

3.3.2. *Batch experiments*

Analyses of cross sections of larger cerussite crystals reacted with the solution (Experiment IIIb) showed that a "crust" was formed, in which individual mimetite crystals were almost palisaded and, in many cases, attached like "teeth" to the substrate (Fig. 5). Probably, the surface of orthorhombic cerussite facilitated heterogeneous nucleation of hexagonal mimetite, but the difference in crystallographic structure was mismatched to allow for epitaxial growth. Therefore, the "crust" was not tight or compact and allowed solution to permeate between separate

crystals for further growth by reaction at the mineral-fluid interface. The evolution of the mimetite "crust" eventually led to the formation of such a uniform but porous layer up to 1 um thick that flaked off in patches revealing the surface of the dissolved cerussite, indicating a weak bonding between the cerussite and the new mimetite phase.

The replacement of cerussite by mimetite occurred only in the outermost parts of the crystal and was not observed in its interior within the time-frame of the experiments (maximum 1 month). EMP WDS analysis of cross-sections did not indicate the presence of As under the layer of mimetite (Fig. 6). "Teeth" of mimetite were characterized by a wide base and they tapered upwards. Cerussite did not dissolve where mimetite adhered to it, but around the "tooth" and there Pb ions were supplied for mimetite growth. This represents the development of a new phase from the initial nanoparticles (probably amorphous) visible in AFM, through crystalline dendrites and needles to hexagonal rods of mimetite.

All these observations indicated that the reaction of cerussite with the solution, leading to the formation of mimetite, occurred on the principle of coupled dissolution-precipitation, however, it led only to a partial pseudomorphic replacement of cerussite by mimetite.

Keeping the fluid transport pathways open to the reaction interface between the primary and product phases is crucial for further progress of the mineral exchange process. There must be generation of porosity in the secondary phase. Two factors are responsible for the initiation of porosity - these are the relative molar volumes of the solid phases and the relative solubilities of the phases in the fluid. The total volume deficit relative to the initial volume of the crystal is the result of combined changes in molar volume and relative solubility. When the final effect of changes in a solid's molar volume and relative solubility is not a volume deficit - no porosity is formed in the secondary phase. Consequently, the reaction proceeds by an interface-coupled dissolution-precipitation mechanism only in the very outer layers of cerussite (Putnis and Putnis, 2007; Pollok et al., 2011).

For low solubility and/or low reactivity environments, such as the lead carbonate and lead arsenate system described herein, Doerner-Hoskins precipitation may be a suitable scenario (Doerner and Hoskins, 1925; Glynn and Reardon, 1990; Pollok et al., 2011). In this system, the successive growth of replacement incremental layers occurs in local equilibrium with the solution at the reaction front. The composition of the solution evolves, the only part in equilibrium with the solution is the most recent replaced part. The condition for the relatively rapid progress of replacement is a negative volume change, followed by the formation of porosity. Positive volume changes, on the other hand, inhibit porosity formation and can lead to passivation of the parent phase, followed by blocking or slowing of the replacement process.

Crystal replacement reactions can be inhibited or retarded by the formation of passivation layers, which reduce the number of surface sites of the original mineral available for further reaction. For instance, the reaction of KCl substrate in KBr solution demonstrates that initial rapid exchange slows down as the reacting surface becomes sealed by an incremental layer, limiting diffusion at the interface (Pollok, 2005; Pollok et al., 2011). Similarly, during the replacement of calcite ($CaCO_3$) by otavite ($CdCO_3$) in cadmium solutions, significant reductions in contaminant concentration are observed initially, but a gradual passivation of the calcite surface occurs, diminishing its capacity to capture further Cd ions (Cubillas et al., 2005; Pérez-Garrido et al., 2007; Julia et al., 2023). A comparable passivation effect is noted in the replacement of magnesium oxide (MgO) with magnesite ($MgCO_3$), where the product layer significantly impedes further reaction after prolonged exposure (Weber et al., 2023). These examples illustrate how the formation of a passivation layer can ultimately slow down coupled dissolution and precipitation processes. Recrystallization of mimetite "crust" and the morphology of product crystals may be also a critical factor causing an armoring of the cerussite substrate and leading to the blockage of the interface-coupled dissolution-precipitation process. Progressive thickening of the overgrowth slowed down the mineral phase transformation. However, the intrinsic intergranular porosity should still be present and the process will not be completely stopped (Morales et al., 2013; Cuesta Mayorga et al., 2018; Forjanes et al., 2020).

To test the effect of Cl deficiency on the products and reaction mechanism (Jonas et al., 2014; Kwaśniak-Kominek, 2018; Manecki et al., 2020), several experiments have been repeated in the absence of Cl^- ions in the system. In this case, cerussite was still capable of removing arsenate from aqueous solutions, and the only product of the mineral replacement reaction was the hydroxyl analog of mimetite: $Pb_5(AsO_4)_3OH$ (hydroxylmimetite). No transitional mineral phases were observed. It was accompanied by schultenite $Pb(HAsO_4)_3$ at pH 2 (Fig. SM 8). The efficiency of As removal was similar: the concentration was reduced from 50 to 0.71 mg As/L within 7 days at pH 2 (Table SM 7). In the latter case even 99 % of As(V) was present in mimetite. The absence of chlorine did not significantly affect the progress of the reaction, the trends in As(V) removal, nor its efficiency. The concentration of Pb released into solution in the pH range of 4–8 was below the detection limit.

Like mimetite, hydroxylmimetite also precipitated as incrustations on cerussite powder crystals, over the entire pH range. The mechanism of the reaction in the absence of Cl^- was similar to the reaction described above. Hydroxylmimetite crystallized in the form of elongated rods and needle-like crystals that were finer than those formed in the presence of Cl^- (Fig. SM 8). The very porous "crust" on the surface of natural cerussite crystal was about 1 μm thick (Fig. SM 9). Microprobe analysis of cross-sections of natural cerussite crystals reacted with arsenate solution for up to 1 month indicated that arsenate is not present in cerussite under the hydroxylmimetite crust (Fig. SM 10). Despite slight differences in the morphology of mimetite and hydroxylmimetite, the nature of the mineral replacement reaction was the same – the partial pseudomorphic replacement of cerussite by a hydroxylmimetite layer was observed.

4. Summary and conclusions

When synthetic cerussite is introduced to water containing arsenate ions, initial reactions reduce arsenate concentrations by more than tenfold. Repeated treatments further enhance the reduction, resulting in over 99 % arsenate removal. The reacted cerussite may also be reused for subsequent treatments. In chloride-containing environments, the primary reaction product was mimetite, $Pb_5(AsO_4)_3Cl$, while in chloride-deficient conditions, a hydroxyl analog formed, with comparable efficiency. Optimal reaction conditions were observed at pH 4–6, where arsenate reduction was maximized, and toxic lead release minimized. At this pH and a concentration of 50 mg/L, the reaction proceeded, resulting in near-complete arsenate removal within days. Additionally, mimetite incrustations can partially coat the cerussite surface, limiting further dissolution and reducing additional lead release. Despite this, the reaction continued at a reduced rate, as shown in multiple-use cerussite powder experiments.

The addition of cations, except for aluminium, did not significantly impact arsenate sequestration at either low (5 mg/L) or high (50 mg/L) initial As concentrations. Similarly, anions had minimal effect, with only sulfate causing a slight reduction in removal efficiency, although this effect was independent of its concentration. In systems containing both cations and anions, arsenate sequestration remained nearly complete (99.5 % to 99.6 %), indicating strong selectivity for As removal, even in multi-ion environments. Experiments with natural thermal waters containing low arsenic levels (0.08–0.1 mg/L) confirmed that arsenate removal proceeds at slower rates, achieving up to 73.8 % reduction over seven days. PHREEQC modelling indicated that when fluoride is present in the waters, it can hinder mimetite precipitation, potentially affecting arsenate sequestration. Additionally, the presence of aluminium was shown to influence arsenate removal, further supporting experimental observations.

Experiments conducted with natural crystals indicated that arsenate

ions are removed through interface-coupled dissolution of cerussite and precipitation of mimetite which incrustates the cerussite surface with distinct crystals. The very low solubility of mimetite guaranteed high efficiency in removing As from solution. Nucleation of mimetite particles was surface controlled, and it precipitated, replacing a cerussite crystal. The forming "crust" partially armoured the surface, but probably it still indicated some intergranular porosity. The effect of armouring might have been larger in the case of natural crystals because they may have greater structural variations (surface roughness) than synthetic powder. Correspondingly, the larger the surface area, the higher the intensity of the reaction and the uptake of As from solution. The results underscored the critical role of dissolution and precipitation processes in mitigating the reactivity of toxic elements in specific polluted environments. Secondary lead phases, such as lead carbonate and lead arsenate, can regulate arsenate and lead concentrations. In various natural and anthropogenic settings, the release of toxic elements into water is governed by dissolution and precipitation processes, e.g. during weathering of minerals.

Removal of arsenate from contaminated waters through reaction with cerussite showed potential as a remediation method. A significant advantage of this method lies in the formation of mimetite ($Pb_5(AsO_4)_3Cl$), a thermodynamically stable product that is poorly soluble across a broad range of pH levels (Magalhães, 2002; Magalhães and Silva, 2003; Bajda, 2010). This stability contrasts sharply with other precipitation methods, such as those involving calcium or ferric arsenates, which can result in less stable products that are more prone to leaching under varying environmental conditions (Langmuir et al., 2006; Zhu et al., 2006; Stefánsson, 2007). As the reaction progresses, cerussite gradually diminishes, while mimetite crystals grow, resulting in a dense, crystalline sediment that is easy to separate from the solution.

Based on the results presented herein and PHREEQC modelling, we conclude that this method could be particularly effective for treating water contaminated with arsenate concentrations exceeding 1 mg As/L, which are commonly observed in acid mine drainage, industrial discharges, and wastewater. However, the reaction rate is influenced by the cerussite-to-solution ratio and the initial arsenate concentration, with the method becoming slower at lower initial concentrations. For arsenate levels below 1 mg/L, the process may be too slow to be practical for treatment applications.

Potential development of the technology applying cerussite for As removal will meet several challenges. Firstly for the method to be efficient all arsenic has to be in the oxidized As(V) state. In certain cases, this may require pretreatment oxidation. Several methods can be employed for the oxidation of arsenite to arsenate. Biological oxidation utilizes specific bacteria, such as Thiomonas and *Acidithiobacillus ferrooxidans*, which are effective in oxidizing arsenite [As(III)] to the less toxic arsenate [As(V)]. This process is particularly beneficial in both natural and engineered environments (Katsoyiannis and Zouboulis, 2004). Another method is ozone oxidation, which has been shown to be highly effective in water treatment applications. Ozone offers rapid reaction rates and minimizes chemical residuals, thereby enhancing the overall efficiency of the treatment process (Kim and Nriagu, 2000). Additionally, hydrogen peroxide serves as a strong oxidizing agent that can convert arsenite to arsenate, especially when used in conjunction with catalysts to improve reaction rates (Hug and Leupin, 2003; Pettine et al., 1999). Manganese and iron compounds are also effective alternatives for oxidizing arsenite to arsenate (Driehaus et al., 1995; Borho and Wilderer, 1996).

An additional consideration is the release of lead (Pb) into the treated solution due to the dissolution of excess cerussite under certain conditions. Lead is a highly toxic metal that poses significant environmental and health risks, making its management crucial in remediation processes. However, this issue can be effectively managed by using established methods for lead immobilization. For instance, the addition of phosphate, such as in the form of hydroxylapatite ($Ca_{10}(PO_4)_6(OH)_2$), facilitates the precipitation of pyromorphite ($Pb_5(PO_4)_3Cl$) in the treatment environment (Ma et al., 1993; Cotter-Howells and Capron, 1996). In our approach, we aim to regulate the pH between 4 and 6 to minimize lead release. Under these conditions, mimetite ($Pb_5(AsO_4)_3Cl$) can form as an incrustation on cerussite, which restricts the dissolution of lead into the solution.

To remove cerussite particles from the water phase after treatment, we propose membrane filtration using 0.20-μm cellulose filters, known for their effective particle retention and compatibility with aqueous solutions. This pore size captures particles above 0.20 μm, minimizing the risk of residual cerussite. We also considered alternative filter materials, such as polypropylene, nylon, or PTFE, for added flexibility in different conditions. This filtration approach ensures the treated water meets safety standards and addresses the potential risks associated with small particle sizes.

The proposed method is a preliminary concept for a series of mobile reactors aimed at addressing arsenate removal from contaminated waters, such as those affected by acid mine drainage or industrial discharges. The initial phase would involve a pretreatment process, including oxidation and the addition of chloride ions, followed by a reaction with cerussite and subsequent filtration. To eliminate any excess lead in the solution, a reaction with phosphate would be implemented, along with additional filtration. The process may also include a liming step with calcium carbonate to remove any remaining pollutants before final filtration through membrane filters. However, this is only an initial idea, and the method will need to be adjusted based on real-world conditions. Additional testing with a broader range of water types and further geochemical modelling is needed to assess its effectiveness in diverse environmental scenarios. The ultimate aim is to develop a laboratory model and conduct tests using contaminated waters to evaluate the effectiveness and feasibility of the proposed treatment strategy.

CRediT authorship contribution statement

Ewa Stępień: Writing – original draft, Visualization, Methodology, Investigation, Funding acquisition, Data curation, Conceptualization. **Maude Julia:** Writing – review & editing, Supervision, Methodology, Investigation, Data curation. **Daniel Buczko:** Writing – review & editing, Supervision, Methodology, Data curation. **Martina Bottaro:** Data curation, Methodology, Supervision, Writing – review & editing. **Andreas Kappler:** Resources, Supervision, Writing – review & editing. **Maciej Manecki:** Writing – review & editing, Visualization, Validation, Supervision, Methodology, Investigation, Data curation, Conceptualization. **Christine V. Putnis:** Writing – review & editing, Validation, Supervision, Resources, Methodology.

Declaration of competing interest

The authors declare that they have no known competing financial interests or personal relationships that could have appeared to influence the work reported in this paper.

Data availability

No data was used for the research described in the article.

Acknowledgements

Funding: Ewa Stępień was supported by the Excellence Initiative – Research University AGH University of Krakow (Action 6: Funding international internships for young employees and doctoral students), Polish National Agency for Academic Exchange PROM Programme (EU Project POWR.03.03.00-IP.08-00-P13/18) and Deutsche Bundesstiftung Umwelt Central and Eastern Europe Fellowship held at the Eberhard-Karls Universität Tübingen (30024/001). Christine V. Putnis and Maude Julia have received funding from the European Union's Horizon 2020 research and innovation programme (FluidNET) under the Marie

Skłodowska-Curie grant agreement No 956127.

We would like to acknowledge Mr. Malte Elsässer and Mr. Carsten Bahr for their assistance in obtaining the natural waters used in the experiments described in this study.

Appendix A. Supplementary data

Supplementary data to this article can be found online at https://doi.org/10.1016/j.chemgeo.2024.122531.

References

Agency for Toxic Substances and Disease Registry (ATSDR), 2024. Toxic Substances List. Accessed October 30, 2024. ATSDR Toxic Substances List.

Alka, S., Shahir, S., Ibrahim, N., Ndejiko, M.J., Vo, D.V.N., Abd Manan, F., 2021. Arsenic removal technologies and future trends: a mini review. J. Clean. Prod. 278, 123805.

Bajda, T., 2010. Solubility of mimetite $Pb_5(AsO_4)_3Cl$ at 5–55 C. Environ. Chem. 7 (3), 268–278.

Bajda, T., Manecki, M., Matyjasik, M., 2019. The early stages of mimetite dissolution in EDTA studied with atomic force microscopy and scanning electron microscopy. Microsc. Microanal. 25 (3), 810–816.

Banning, A., 2021. Geogenic arsenic and uranium in Germany: Large-scale distribution control in sediments and groundwater. J. Hazard. Mater. 405, 124186.

Biswas, A., Gustafsson, J.P., Neidhardt, H., Halder, D., Kundu, A.K., Chatterjee, D., Bhattacharya, P., 2014. Role of competing ions in the mobilization of arsenic in groundwater of Bengal Basin: insight from surface complexation modeling. Water Res. 55, 30–39.

Borho, M., Wilderer, P., 1996. Optimized removal of arsenate (III) by adaptation of oxidation and precipitation processes to the filtration step. Water Sci. Technol. 34 (9), 25–31.

Bothe, J.V., Brown, P.W., 1999. Arsenic immobilization by calcium arsenate formation. Environ. Sci. Technol. 33 (21), 3806–3811.

Brown, P.L., Sylva, R.N., Batley, G.E., Ellis, J., 1985. The hydrolysis of metal ions. Part 8. Aluminium (III). J. Chem. Soc. Dalton Trans. 9, 1967–1970.

Campbell, K.M., Nordstrom, D.K., 2014. Arsenic speciation and sorption in natural environments. Rev. Mineral. Geochem. 79 (1), 185–216.

Cheng, H., Hu, Y., Luo, J., Xu, B., Zhao, J., 2009. Geochemical processes controlling fate and transport of arsenic in acid mine drainage (AMD) and natural systems. J. Hazard. Mater. 165 (1–3), 13–26.

Chernov, A.A., 1984. Growth mechanisms. In: Modern Crystallography III: Crystal Growth, pp. 104–158.

Cotter-Howells, J., Capron, S., 1996. Remediation of contaminated land by formation of heavy metal phosphates. Appl. Geochem. 11 (1–2), 335–342.

Cubillas, P., Köhler, S., Prieto, M., Causserand, C., Oelkers, E.H., 2005. How do mineral coatings affect dissolution rates? An experimental study of coupled $CaCO_3$ dissolution—$CdCO_3$ precipitation. Geochim. Cosmochim. Acta 69 (23), 5459–5476.

Cuesta Mayorga, I., Astilleros, J.M., Fernández-Díaz, L., Morales, J., Prieto, M., Roncal-Herrero, T., Benning, L.G., 2018. Epitactic overgrowths of calcite ($CaCO_3$) on anhydrite ($CaSO_4$) cleavage surfaces. Cryst. Growth Des. 18 (3), 1666–1675.

Darland, J.E., Inskeep, W.P., 1997. Effects of pH and phosphate competition on the transport of arsenate. Am. Soc. Agron. Crop Sci. Soc. Am. Soil Sci. Soc. Am. 26 (4), 1133–1139.

Doerner, H.A., Hoskins, W.M., 1925. Co-precipitation of radium and barium sulfates. J. Am. Chem. Soc. 47 (3), 662–675.

Drahota, P., Filippi, M., 2009. Secondary arsenic minerals in the environment: a review. Environ. Int. 35 (8), 1243–1255.

Driehaus, W., Reiner, S., Jekel, M., 1995. Oxidation of arsenate (III) with manganese oxides in water treatment. Water Res. 29 (1), 297–305.

Dzombak, D.A., Morel, F.M., 1991. Surface Complexation Modelling: Hydrous Ferric Oxide. John Wiley & Sons.

Fernandez-Diaz, L., Pina, C.M., Astilleros, J.M., Sanchez-Pastor, N., 2009. The carbonatation of gypsum: pathways and pseudomorph formation. Am. Mineral. 94 (8–9), 1223–1234.

Flis, J., Manecki, M., Bajda, T., 2011. Solubility of pyromorphite $Pb_5(PO_4)_3Cl$–mimetite $Pb_5(AsO_4)_3Cl$ solid solution series. Geochim. Cosmochim. Acta 75 (7), 1858–1868.

Forjanes, P., Astilleros, J.M., Fernández-Díaz, L., 2020. The formation of barite and celestite through the replacement of gypsum. Minerals 10 (2), 189.

Ghosh, A., Sáez, A.E., Ela, W., 2006. Effect of pH, competitive anions and NOM on the leaching of arsenic from solid residuals. Sci. Total Environ. 363 (1–3), 46–59.

Glynn, P.D., Reardon, E.J., 1990. Solid-solution aqueous-solution equilibria; thermodynamic theory and representation. Am. J. Sci. 290 (2), 164–201.

Gołębiowska, B., Pieczka, A., Franus, W., 2002. Ca-bearing phosphatian mimetite from Rędziny, Lower Silesia, Poland. Neues Jahrbuch für Mineralogie-Monatshefte 31–41.

Horcas, I., Fernandez, R., Gomez-Rodriguez, J.M., Colchero, J., Gomez-Herrero, J., Baro, A.M., 2007. WSXM: a software for scanning probe microscopy and a tool for nanotechnology. Rev. Sci. Instrum. 78, 013705.

Hug, S.J., Leupin, O., 2003. Iron-catalysed oxidation of arsenic (III) by oxygen and by hydrogen peroxide: pH-dependent formation of oxidants in the Fenton reaction. Environ. Sci. Technol. 37 (12), 2734–2742.

Hughes, J.M., Rakovan, J.F., 2015. Structurally robust, chemically diverse: apatite and apatite supergroup minerals. Elements 11 (3), 165–170.

Jonas, L., John, T., King, H.E., Geisler, T., Putnis, A., 2014. The role of grain boundaries and transient porosity in rocks as fluid pathways for reaction front propagation. Earth Planet. Sci. Lett. 386, 64–74.

Julia, M., Putnis, C.V., King, H.E., Renard, F., 2023. Coupled dissolution-precipitation and growth processes on calcite, aragonite, and Carrara marble exposed to cadmium-rich aqueous solutions. Chem. Geol. 621, 121364.

Kartinen Jr., E.O., Martin, C.J., 1995. An overview of arsenic removal processes. Desalination 103 (1–2), 79–88.

Kasioptas, A., Geisler, T., Perdikouri, C., Trepmann, C., Gussone, N., Putnis, A., 2011. Polycrystalline apatite synthesized by hydrothermal replacement of calcium carbonates. Geochim. Cosmochim. Acta 75 (12), 3486–3500.

Katsoyiannis, I.A., Zouboulis, A.I., 2004. Application of biological processes for the removal of arsenic from groundwaters. Water Res. 38 (1), 17–26.

Kim, M.J., Nriagu, J., 2000. Oxidation of arsenite in groundwater using ozone and oxygen. Sci. Total Environ. 247 (1), 71–79.

Kwaśniak-Kominek, M., 2018. The Mechanisms of Formation of Pyromorphite in the Presence of Cerussite. Doctoral dissertation.. AGH University of Science and Technology in Kraków.

Langmuir, D., Mahoney, J., Rowson, J., 2006. Solubility products of amorphous ferric arsenate and crystalline scorodite (FeAsO4· 2H2O) and their application to arsenic behavior in buried mine tailings. Geochim. Cosmochim. Acta 70 (12), 2942–2956.

Laperche, V., Logan, T.J., Gaddam, P., Traina, S.J., 1997. Effect of apatite amendments on plant uptake of lead from contaminated soil. Environ. Sci. Technol. 31 (10), 2745–2753.

Lenoble, V., Deluchat, V., Serpaud, B., Bollinger, J.C., 2003. Arsenite oxidation and arsenate determination by the molybdene blue method. Talanta 61 (3), 267–276.

Lu, P., Zhang, G., Apps, J., Zhu, C., 2022. Comparison of thermodynamic data files for PHREEQC. Earth Sci. Rev. 225, 103888.

Lytle, D.A., Sorg, T.J., Snoeyink, V.L., 2005. Optimizing arsenic removal during iron removal: theoretical and practical considerations. J. Water Supply Res. Technol. AQUA 54 (8), 545–560.

Ma, Q.Y., Traina, S.J., Logan, T.J., Ryan, J.A., 1993. In situ lead immobilization by apatite. Environ. Sci. Technol. 27 (9), 803–1810.

Ma, Q.Y., Logan, T.J., Traina, S.J., Ryan, J.A., 1994. Effects of NO^{3-}, Cl^-, F^-, SO_4^{2-}, and CO_3^{2-}on Pb^{2+} immobilization by hydroxyapatite. Environ. Sci. Technol. 28 (3), 408–418.

Ma, Q.Y., Traina, S.J., Logan, T.J., Ryan, J.A., 1994b. Effects of aqueous Al, Cd, Cu, Fe (II), Ni, and Zn on Pb immobilization by hydroxyapatite. Environ. Sci. Technol. 28 (7), 1219–1228.

Ma, Q.Y., Logan, T.J., Traina, S.J., 1995. Lead immobilization from aqueous solutions and contaminated soils using phosphate rocks. Environ. Sci. Technol. 29 (4), 1118–1126.

Magalhães, M.C.F., 2002. Arsenic. An environmental problem limited by solubility. Pure Appl. Chem. 74 (10), 1843–1850.

Magalhães, M.C.F., Silva, M.C.M., 2003. Stability of lead (II) arsenates. Monatshefte fuer Chemie/Chemical Monthly 134, 735–743.

Manecki, M., 2019. Lead in water and soil - speciation toxicity and treatment technologies. In: Encyclopedia of Water: Science, Technology, and Society, pp. 1–13.

Manecki, M., Maurice, P.A., Traina, S.J., 2000. Uptake of aqueous Pb by Cl^-, F^-, and OH^- apatites: mineralogic evidence for nucleation mechanisms. Am. Mineral. 85 (7–8), 932–942.

Manecki, M., Kwaśniak-Kominek, M., Majka, J., Rakovan, J., 2020. Model of interface-coupled dissolution-precipitation mechanism of pseudomorphic replacement reaction in aqueous solutions based on the system of cerussite $PbCO_3$–pyromorphite $Pb_5 (PO_4)_3Cl$. Geochim. Cosmochim. Acta 289, 1–13.

Manning, B.A., Goldberg, S., 1996. Modeling competitive adsorption of arsenate with phosphate and molybdate on oxide minerals. Soil Sci. Soc. Am. J. 60 (1), 121–131.

Manning, B.A., Goldberg, S., 1997. Adsorption and stability of arsenic (III) at the clay mineral– water interface. Environ. Sci. Technol. 31 (7), 2005–2011.

Marciniak, H., Diduszko, R., Kozak, M., 2006. XRAYAN Program do Rentgenowskiej Analizy Fazowej, Wersja 4.0.1. Koma.

Migaszewski, Z.M., Gałuszka, A., Dołęgowska, S., 2018. Arsenic in the Wiśniówka acid mine drainage area (south-central Poland)–mineralogy, hydrogeochemistry, remediation. Chem. Geol. 493, 491–503.

Mohan, D., Pittman, C.U., 2007. Arsenic removal from water/wastewater using adsorbents—a critical review. J. Hazard. Mater. 142 (1–2), 1–53.

Mohanty, D., 2017. Conventional as well as emerging arsenic removal technologies—a critical review. Water Air Soil Pollut. 228 (10), 381.

Morales, J., Astilleros, J.M., Fernández-Díaz, L., Álvarez-Lloret, P., Jiménez, A., 2013. Anglesite ($PbSO_4$) epitactic overgrowths and substrate-induced twinning on anhydrite (CaSO4) cleavage surfaces. J. Cryst. Growth 380, 130–137.

Murcott, S., 2012. Arsenic Contamination in the World. IWA Publishing.

Nicomel, N., Leus, K., Folens, K., Van Der Voort, P., Du Laing, G., 2015. Technologies for arsenic removal from water: current status and future perspectives. Int. J. Environ. Res. Public Health 13 (1), 62.

Nordstrom, D.K., Alpers, C.N., 1999. Negative pH, efflorescent mineralogy, and consequences for environmental restoration at the Iron Mountain Superfund site, California. Proc. Natl. Acad. Sci. 96 (7), 3455–3462.

Paikaray, S., 2015. Arsenic geochemistry of acid mine drainage. Mine Water Environ. 34 (2), 181–196.

Parkhurst, D.L., Appelo, C.A.J., 1999. User's guide to PHREEQC (Version 2): a computer program for speciation, batch-reaction, one-dimensional transport, and inverse geochemical calculations. Water-Resources Investigations Report 99 (4259), 312.

Pérez-Garrido, C., Fernández-Díaz, L., Pina, C.M., Prieto, M., 2007. In situ AFM observations of the interaction between calcite ($10\bar{1}4$) surfaces and Cd-bearing aqueous solutions. Surf. Sci. 601 (23), 5499–5509.

Pettine, M., Campanella, L., Millero, F.J., 1999. Arsenite oxidation by H_2O_2 in aqueous solutions. Geochim. Cosmochim. Acta 63 (18), 2727–2735.
Pierce, M.L., Moore, C.B., 1982. Adsorption of arsenite and arsenate on amorphous iron hydroxide. Water Res. 16 (7), 1247–1253.
Plumlee, G.S., Smith, K.S., Montour, M.R., Ficklin, W.H., Mosier, E.L., 1997. Geologic Controls on the Composition of Natural Waters and Mine Waters Draining Diverse Mineral-Deposit Types.
Pokrovsky, O.S., Schott, J., 2002. Surface chemistry and dissolution kinetics of divalent metal carbonates. Environ. Sci. Technol. 36 (3), 426–432.
Pollok, K., 2005. Crystal Growth Patterns in Solid Solution Systems: Case Studies on Oscillatory Zoning and Mineral Replacement Reactions. Doctoral dissertation. Westfälische Wilhelms-Universität Münster.
Pollok, K., Putnis, C.V., Putnis, A., 2011. Mineral replacement reactions in solid solution-aqueous solution systems: volume changes, reactions paths and end-points using the example of model salt systems. Am. J. Sci. 311 (3), 211–236.
Putnis, A., 2002. Mineral replacement reactions: from macroscopic observations to microscopic mechanisms. Miner. Mag. 66, 689–708.
Putnis, A., 2009. Mineral replacement reactions. Rev. Mineral. Geochem. 70 (1), 87–124.
Putnis, A., Putnis, C.V., 2007. The mechanism of reequilibration of solids in the presence of a fluid phase. J. Solid State Chem. 180 (5), 1783–1786.
Putnis, C.V., Putnis, A., 2022. A mechanism of ion exchange by interface-coupled dissolution-precipitation in the presence of an aqueous fluid. J. Cryst. Growth 600, 126840.
Putnis, C.V., Ruiz-Agudo, E., 2013. The mineral–water interface: where minerals react with the environment. Elements 9 (3), 177–182.
Putnis, C.V., Renard, F., King, H.E., Montes-Hernandez, G., Ruiz-Agudo, E., 2013. Sequestration of selenium on calcite surfaces revealed by nanoscale imaging. Environ. Sci. Technol. 47 (23), 13469–13476.
Renard, F., Putnis, C.V., Montes-Hernandez, G., Ruiz-Agudo, E., Hovelmann, J., Sarret, G., 2015. Interactions of arsenic with calcite surfaces revealed by in situ nanoscale imaging. Geochim. Cosmochim. Acta 159, 61–79.
Renard, F., Putnis, C.V., Montes-Hernandez, G., King, H.E., 2017. Siderite dissolution coupled to iron oxyhydroxide precipitation in the presence of arsenic revealed by nanoscale imaging. Chem. Geol. 449, 123–134.
Romero, F.M., Prol-Ledesma, R.M., Canet, C., Alvares, L.N., Pérez-Vázquez, R., 2010. Acid drainage at the inactive Santa Lucia mine, western Cuba: natural attenuation of arsenic, barium and lead, and geochemical behavior of rare earth elements. Appl. Geochem. 25 (5), 716–727.
Ruiz-Agudo, E., Kowacz, M., Putnis, C.V., Putnis, A., 2010. The role of background electrolytes on the kinetics and mechanism of calcite dissolution. Geochim. Cosmochim. Acta 74 (4), 1256–1267.
Ruiz-Agudo, E., Putnis, C.V., Putnis, A., 2014. Coupled dissolution and precipitation at mineral–fluid interfaces. Chem. Geol. 383, 132–146.
Sahai, N., Schoonen, M.A., 2020. Accuracy of thermodynamic databases for hydroxyapatite dissolution constant. Astrobiology 20 (1), 157–160.
Smedley, P.L., Kinniburgh, D.G., 2002. A review of the source, behaviour and distribution of arsenic in natural waters. Appl. Geochem. 17 (5), 517–568.
Sordyl, J., Rybka, K., Dziewiątka, K., Jędras, A., Skalny, M., Staszel, K., Manecki, M., 2022. The influence of the synthesis procedure on the morphology of REE-enriched Pb-apatite (pyromorphite). EGU General Assembly Conference Abstracts EGU22–7905.
Sorg, T.J., Logsdon, G.S., 1978. Treatment technology to meet the interim primary drinking water regulations for inorganics: part 2. J. - Am. Water Works Assoc. 70 (7), 379–393.
Stefánsson, A., 2007. Iron (III) hydrolysis and solubility at 25 C. Environ. Sci. Technol. 41 (17), 6117–6123.
Stumm, W., Morgan, J.J., 1985. Aquatic Chemistry. Wiley, New York.
Stumm, W., Morgan, J.J., 2013. Aquatic Chemistry: Chemical Equilibria and Rates in Natural Waters. John Wiley & Sons.
Turek, P., Bajda, T., Manecki, M., 2015. Dissolution of mimetite $Pb_5(AsO_4)_3Cl$ in malic acid solutions. Mineralogia 45 (1–2), 3.
Voigt, M., Marieni, C., Clark, D.E., Gíslason, S.R., Oelkers, E.H., 2018. Evaluation and refinement of thermodynamic databases for mineral carbonation. Energy Procedia 146, 81–91.
Wang, Q.W., Morse, J.W., 1996. Pyrite formation under conditions approximating those in anoxic sediments. Pathway and morphology. Mar. Chem. 52, 99–121.
Wang, L., Putnis, C.V., Ruiz-Agudo, E., King, H.E., Putnis, A., 2013. Coupled dissolution and precipitation at the cerussite-phosphate solution interface: Implications for immobilization of lead in soils. Environ. Sci. Technol. 47 (23), 13502–13510.
Weber, J., Starchenko, V., Yuan, K., Anovitz, L.M., Ievlev, A.V., Unocic, R., Borisevich, A. Y., Boebinger, M.G., Stack, A.G., 2023. Armoring of MgO by a passivation layer impedes direct air capture of CO_2. Environ. Sci. 57 (40), 14929–14937.
Xu, Y., Schwartz, F.W., 1994. Lead immobilization by hydroxyapatite in aqueous solutions. J. Contam. Hydrol. 15 (3), 187–206.
Zhu, Y.N., Zhang, X.H., Xie, Q.L., Wang, D.Q., Cheng, G.W., 2006. Solubility and stability of calcium arsenates at 25◦ C. Water Air Soil Pollut. 169, 221–238.